Journal Pre-proof

Topological centrality and spatial advantage in the competition between networks

Paula Rodríguez-Sánchez, Johann H. Martínez, Javier M. Buldú

PII: S0378-4371(26)00934-9
DOI: https://doi.org/10.1016/j.physa.2026.132188
Reference: PHYSA 132188

To appear in: *Physica A*

Please cite this article as: P. Rodríguez-Sánchez, J.H. Martínez and J.M. Buldú, Topological centrality and spatial advantage in the competition between networks, *Physica A* (2026), doi: https://doi.org/10.1016/j.physa.2026.132188.

This is a PDF of an article that has undergone enhancements after acceptance, such as the addition of a cover page and metadata, and formatting for readability. This version will undergo additional copyediting, typesetting and review before it is published in its final form. As such, this version is no longer the Accepted Manuscript, but it is not yet the definitive Version of Record; we are providing this early version to give early visibility of the article. Please note that Elsevier's sharing policy for the Published Journal Article applies to this version, see: https://www.elsevier.com/about/policies-and-standards/sharing#4-published-journal-article. Please also note that, during the production process, errors may be discovered which could affect the content, and all legal disclaimers that apply to the journal pertain.

© 2026 Published by Elsevier B.V.

Journal Pre-proof

Revised manuscript (marked up)

Click here to view linked References

Topological centrality and spatial advantage in the competition between networks

Paula Rodríguez-Sánchez, Johann H. Martínez, Javier M. Buldú

Complex Systems Group & G.I.S.C., King Juan Carlos University, Móstoles 28933, Spain

Abstract

Networks rarely compete in isolation. Firms, infrastructures, biological populations, social groups, and institutions interact with rivals while being embedded in physical or functional spaces. Previous work on competing networks has shown that the outcome of a linear spreading process depends on the spectral properties of the interacting networks and on the centrality of the connector nodes. However, these models usually assume that all nodes of a network have the same ability to exploit the interaction once the inter-network link is created, disregarding spatial limitations. Here we introduce a spatial extension of the competing-networks framework in which two networks occupy adjacent regions separated by a boundary. The key ingredient is an energy vector assigned to the nodes, whose components decrease with the Euclidean distance to the boundary. This vector transforms the evolution operator of the system and couples topology with space. Now, a node is not only important because of its topological position, but also because of its spatial access to the competing region. Using pairs of Barabási–Albert networks, we compare central–central and peripheral–peripheral connection strategies while progressively relocating the nodes of the weaker network with respect to the boundary. We show that a topologically weaker network can overtake a stronger competitor when its most central nodes are placed sufficiently close to the boundary, whereas placing only peripheral nodes near the boundary is typically insufficient except under extreme spatial sensitivity. We also develop an analytical treatment of how the difference in spectral strength between the two competing networks affects the transition, obtaining results that agree with the numerical simulations.

1. Introduction

The study of complex networks has progressively moved from isolated graphs to systems composed of multiple interacting networks. This shift is necessary because many real systems are not organized as a single set of equivalent interactions, but as networks of networks, interdependent networks, multiplex systems, or multilayer architectures in which different subsystems influence one another through a limited number of coupling relations [1, 2, 3, 4]. In such

Journal Pre-proof

Journal Pre-proof

settings, the properties of the whole system cannot be inferred by analysing each layer or subsystem separately. Inter-network dependencies may amplify failures, modify robustness, change spreading pathways, alter synchronization properties, and generate collective behaviour that has no counterpart in isolated networks [1, 2, 4]. Recent reviews have summarized how this perspective has been extended to the structure, dynamics, robustness, and resilience of interconnected systems [5, 6].

Within this broader framework, a particular line of research has focused on networks that compete for a common resource. Aguirre, Papo and Buldú showed that the result of a competition between two networks can be predicted from spectral properties of the coupled system and, in particular, from the eigenvector centrality of the nodes selected to connect the networks [7]. In that framework, two networks are coupled by one or several connector links and a linear dynamical process evolves on the resulting network of networks. The network that accumulates the largest fraction of the asymptotic population is interpreted as the winner of the competition. Later work extended this perspective by considering out-of-equilibrium dynamics and showing that the connector strategy also determines the time needed to reach the asymptotic regime [8]. Interestingly, depending on whether the goal is to maximize the final accumulated population, to accelerate convergence, or to delay an unfavourable equilibrium, the optimal inter-network connection may involve central or peripheral nodes. The framework has also been used to show that networks with a smaller leading eigenvalue can survive, or even prevail, when they connect strategically [9], to model the formation of complex socioeconomic structures driven by centrality-based interests [10], and, more recently, to analyse multipolarity in global geopolitics [11]. In a related direction, dynamic interdependence and competition between the layers of multilayer networks have been shown to give rise to abrupt transitions and multistability [12].

To make these notions precise, it is useful to summarize the three ingredients of the competing-networks framework that we adopt here. (i) *Competing networks*: two networks, each with its own internal topology, are joined by a small number of connector links, or interlinks, so that they form a single network-of-networks. (ii) *Dynamical rule*: a non-negative quantity, which may represent a population, a resource, or an influence, is propagated linearly, so that at each time step every node receives the quantity held by its neighbours. After normalization, the state of the system converges to the dominant eigenvector of the evolution operator, whose components are the eigenvector centralities of the nodes [13, 7]. (iii) *Outcome of the competition*: the fraction of this asymptotic quantity accumulated by each network, i.e. the sum of the eigenvector centralities of its nodes, defines its share of the system, and the network that gathers more than one half of it is considered the winner [7]. In the absence of other effects, the network with the largest leading eigenvalue tends to win. However, the outcome also depends on which nodes are used as connectors. Depending on the connector strategy, the dominant eigenvector can be shared between the two networks or localized almost entirely in one of them, giving rise to winner-takes-all outcomes [7, 8]. Localization of the principal eigenvector, and its sensitivity

Journal Pre-proof

to small structural changes, has been extensively characterized in single networks [14, 15, 16, 17]. In multiplex networks, the leading eigenvector can switch from being localized in one layer to being delocalized as the inter-layer coupling increases [18, 19], a phenomenon closely related to the two-mode description developed in this work.

However, competition between real networks is rarely purely topological. Networks are often embedded in space and their nodes have positions, territories, accessibility constraints, or distances to relevant interfaces. Spatial constraints are known to affect the architecture and dynamics of networks because space introduces costs, local constraints, anisotropies, and distance-dependent interactions [20] (see also Ref. [21]). Classical spatial network models, such as Waxman graphs and random geometric graphs, explicitly couple topology to geometry [22, 23]. More applied examples include models of distribution and transportation networks, which consider trade-offs between wiring cost and efficiency [24]. Under this framework, studies of coupled spatial networks have shown that transport performance depends on both the coupling between systems and the spatial distribution of sources and sinks [25]. More recently, spatial interdependent networks have been shown to display transitions whose nature depends on the spatial range of the dependency couplings [26], and two spatially adjacent superconducting networks coupled across an interface have provided an experimental realization of interdependent networks [27]. Boundaries themselves are known to strongly affect the properties of spatially embedded networks, for instance by dominating the connectivity of confined random geometric graphs [28, 29]. Spatial embedding is also a confounder in community detection and other mesoscale analyses, because part of the observed structure may be explained by distance rather than by purely topological organization [30]. Despite this rich literature, the specific problem of how two spatially embedded networks compete when their interaction is mediated by a boundary remains much less explored.

The two lines of research summarized above therefore leave a specific gap. On the one hand, the competing-networks framework identifies topology and connector centrality as the determinants of the winner, but implicitly assumes that all nodes are equally able to receive and retain the propagated quantity, regardless of where they are located. A network that is weaker in spectral terms is, within this description, condemned to lose unless the connector strategy is changed. On the other hand, spatial network models mainly use geometry to determine which links exist and how costly they are, rather than to modulate the dynamical capacity of the nodes that compete through a common interface. As a consequence, it remains unclear whether, and under which conditions, a favourable spatial position can compensate for a topological disadvantage. This is the question addressed in this work.

This gap is relevant in many contexts. Regions, institutions, firms, biological populations, or technological infrastructures may occupy different spatial domains and interact through an interface. In these cases, proximity to the border can be interpreted as access to the competitor, exposure to an external environment, ability to capture incoming resources, or sensitivity to cross-boundary

Journal Pre-proof

influence. Therefore, a node close to the border may have a competitive advantage even if it is not the most central node of its own network. Conversely, a structurally important node located far from the interface may be unable to exploit the interaction efficiently.

Here we introduce a minimal model for the competition of two spatial networks separated by a border. Our model extends the spectral framework of competing networks by assigning an energy value to each node as a function of its distance to the boundary. The resulting energy vector transforms the evolution operator of the coupled system, so that the outcome of the competition depends simultaneously on node centrality, connector strategy, and spatial position. We study two networks with the same number of nodes, initially chosen such that network A is topologically stronger than network B according to their largest eigenvalues. The networks are embedded in two adjacent regions of a two-dimensional domain and connected through either their most central nodes or their most peripheral nodes. We then progressively reorganize the spatial configuration of the weaker network B, placing either its central or peripheral nodes closer to the border, and quantify how this affects the accumulated centrality, the spatial dispersion of the global centrality, and the time required to reach equilibrium. In addition to the simulations, we project the spatially weighted operator onto the leading modes of the two uncoupled networks. This reduced description gives an explicit condition for the dominance reversal and a parameter-free prediction of the spatial threshold, which we test directly against the numerical simulations. Our model shows that, under the appropriate conditions, space can reverse the outcome expected from topology alone. A weaker network may defeat a stronger one if its structurally relevant nodes are positioned close enough to the boundary and if the spatial energy decays sufficiently fast with distance. The energy-vector formulation is deliberately general and, although we focus on distance to a border, the same mechanism can encode other node-specific attributes such as age, activity, infrastructure capacity, degradation, or local learning potential.

In summary, the contributions of this work are threefold. First, we introduce an energy-weighted evolution operator that couples the topological centrality of the nodes with their distance to the boundary, while leaving the topology of the networks unchanged. Second, we show numerically that the alignment between centrality and spatial accessibility, rather than proximity to the boundary alone, determines whether the topologically weaker network can win, and that the connector strategy controls whether the reversal is smooth (CC) or abrupt (PP). Third, we derive a two-mode analytical condition that predicts the spatial threshold for the reversal in individual realizations. The rest of the paper is organized as follows. Section 2 describes the model, the outcome measures, and the analytical approximation. Section 3 presents the results for the CC and PP strategies and compares the analytical and numerical thresholds. Finally, Section 4 discusses the implications and limitations of the model.

Journal Pre-proof

2. Methods

2.1. Competing networks and connector strategies

We consider two binary networks, A and B, with adjacency matrices G_A and G_B and the same number of nodes, $N_A = N_B = N$. For each realization, the isolated networks are labelled so that

$$\lambda_{A,1} > \lambda_{B,1}, \tag{1}$$

where $\lambda_{A,1}$ and $\lambda_{B,1}$ are the largest eigenvalues of G_A and G_B, respectively. Following previous work on competing networks [7, 8], network A is therefore referred to as the *strong network* and network B as the *weak network*.

The two networks are coupled by a single undirected connector link, also called the *interlink*. We analyse two canonical strategies. In the central–central (CC) strategy, the interlink joins the node with the highest eigenvector centrality in A to the node with the highest eigenvector centrality in B. In the peripheral–peripheral (PP) strategy, the interlink joins the node with the lowest eigenvector centrality in each network. The centrality values used to select connector nodes are computed in the isolated networks, before the interlink is added [13, 7]. Once networks are connected, the adjacency matrix of the coupled system is

$$M = \begin{pmatrix} G_A & C \\ C^\top & G_B \end{pmatrix}, \tag{2}$$

where the elements of C are zero with the exception of the element corresponding to the interlink, which is set to one. The total number of nodes of this *network-of-networks* is $N_T = N_A + N_B = 2N$. In all our simulations, we set $N_A = N_B = 100$.

2.2. Spatial embedding and spatial configuration parameter

Without loss of generality, the coupled system is embedded in a two-dimensional Euclidean domain $[0, 100] \times [0, 100]$. Importantly, a vertical boundary at

$$x_b = 50 \tag{3}$$

separates the two spatial regions. Network A occupies the left region, $0 \leq x < x_b$, and network B the right region, $x_b < x \leq 100$.

As a consequence of embedding the networks in space, the number of possible coupling strategies increases. In a non-spatial setting, the selection of the connector nodes can only rely on their topological role within each network. This naturally leads to two limiting strategies, namely connecting either the most central nodes or the most peripheral ones. Once a spatial coordinate is assigned to every node and the two networks are separated by a boundary, an additional and independent criterion becomes available. Connector nodes can now also be selected according to their distance from the boundary. Figure 1(a) therefore illustrates four limiting connection criteria. Strategy L1 connects the most central node of each network, whereas L2 connects the most peripheral

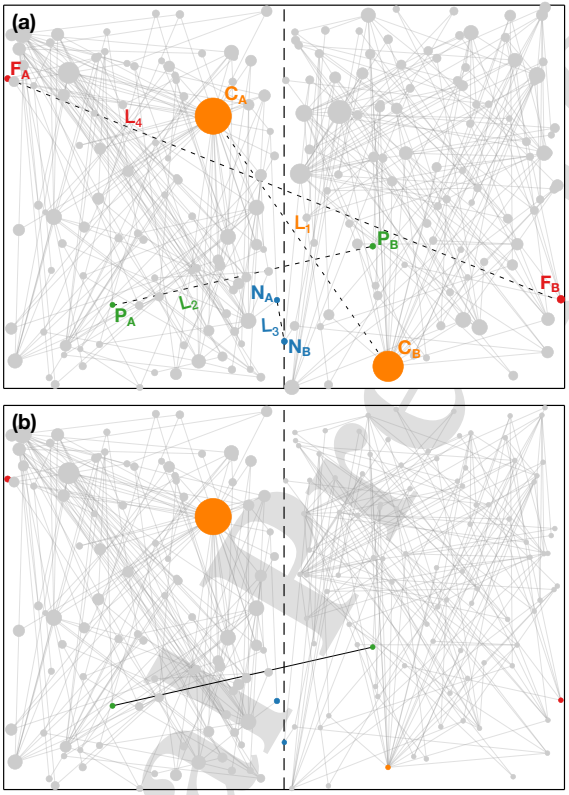

Figure 1: Two competing networks partitioned by a boundary. **(a)** Disconnected state, where node size reflects local eigenvector centrality. The dashed lines denote the four limiting connection criteria: connecting the most central nodes (L1), the most peripheral nodes (L2), the nodes nearest to the boundary (L3), and the nodes farthest from the boundary (L4). **(b)** Connected system, where node size represents global eigenvector centrality. In this example, the two networks are connected through their most peripheral nodes (L2). We can observe how the strong network (on the left) accumulates the majority of the centrality of the connected system. This is a consequence of the localization of the dominant eigenvector produced by PP coupling: the nodes of network A keep sizes very similar to those of panel (a), whereas the centrality of all nodes of network B is strongly suppressed, so that they appear with small and nearly uniform sizes. This winner-takes-all localization is the typical outcome of PP coupling [7]. A quantitative representation of the centrality of individual nodes is given in Figs. S10 and S11 of the Supplementary Information. In this representation, both networks consist of $N_A = N_B = 100$ nodes. Node colors indicate their topological or spatial roles: orange represents the most topologically central nodes, green the most topologically peripheral nodes, red the nodes farthest from the boundary, and blue the nodes closest to the boundary.

Journal Pre-proof

ones. These two strategies are defined exclusively by the network topology. By contrast, L3 connects the nodes nearest to the boundary, while L4 connects those farthest from it, and are therefore defined exclusively by spatial position. In the simulations below, these spatial extremes are explored continuously through the variation of the spatial parameter s, rather than treated as independent connector strategies. Importantly, topological relevance and spatial proximity do not necessarily coincide. A highly central node may be located far from the boundary, whereas a peripheral node may be the closest one to the competing network. These four limiting criteria consequently allow us to disentangle the effects of topological importance and spatial accessibility on the outcome of the competition. In the figure, node size represents global eigenvector centrality. Figure 1(b) shows an example of the distribution of centrality when the interlink connects the two peripheral nodes of these networks (L2 strategy). In this case, the dominant eigenvector is localized in the strong network: the centrality of the nodes of A is almost unaffected by the coupling, while all nodes of B have a strongly suppressed centrality, which explains their small and nearly uniform sizes in the figure.

Because we are concerned about spatial effects on the distance to the boundary, the relevant coordinate is x, and the distance of node i to the boundary is

$$d_i = |x_i - x_b|. \tag{4}$$

To facilitate the interpretation of the results, network A is kept fixed throughout the analysis, with all its nodes located at $x = 25$, and therefore at distance $d_i = 25$ from the boundary. The spatial organization of network B is controlled by the *spatial parameter* $s \in [-25, 25]$. This parameter controls the spatial displacement of the nodes of network B from the coordinate $x = 75$, which corresponds to a spatial configuration symmetric to network A. Therefore, at the reference configuration $s = 0$, all nodes of B are located at $x = 75$, also at distance 25 from the boundary.

The absolute value $|s|$ controls the degree to which network B is dispersed away from this reference configuration, whereas the sign of s determines the alignment between topological centrality and proximity to the boundary. For $s > 0$, nodes are progressively ordered along the x-axis according to their eigenvector-centrality ranking, with the most central nodes moving towards the boundary and the most peripheral nodes moving towards the outer edge of the region. In cases where multiple nodes share identical initial centrality values, ties are broken based on their original numerical index to ensure unique spatial ranking. At the maximally ordered configuration, $s = 25$, the most central node is located at $x = 50 + \delta_x$, where $\delta_x = 0.001$ prevents direct contact with the boundary, whereas the most peripheral node is close to $x = 100 - \delta_x$. For $s < 0$, this ordering is reversed. Peripheral nodes move towards the boundary and central nodes move away from it, so that at $s = -25$ the most peripheral node is closest to the boundary and the most central node is farthest away. Intermediate values of $|s|$ progressively interpolate between the reference configuration and the corresponding maximally ordered arrangement. Specifically,

Journal Pre-proof

the x-coordinate of each node at an intermediate value s is obtained by linearly interpolating between its position at the reference configuration ($x = 75$) and its corresponding target position at $s = 25$ (or $s = -25$), using $|s|/25$ as the interpolation factor. At $s = \pm 25$, the target positions are equally spaced in centrality rank: the half of the nodes favoured by the sign of s are placed between the boundary and $x = 75$, and the other half between $x = 75$ and the outer edge of the region. In the numerical simulations, the values of s are modified in steps of $\Delta s = 0.5$, resulting in 101 discrete spatial configurations.

2.3. Distance-dependent energy and spatially modulated dynamics

The central assumption of our spatial model is that the effective energy of a node depends on its distance to the boundary. We first define the unnormalized spatial weight [31]

$$\widetilde{e}_i = \exp(-\beta d_i), \tag{5}$$

where $\beta \geq 0$ controls the spatial sensitivity to distance from the boundary. When $\beta = 0$, all nodes have the same energy and the competition is determined by topology alone, up to a global multiplicative factor. As β increases, the energy of the nodes decays more rapidly with distance, and proximity to the boundary becomes increasingly important. Therefore, we will call β the *energy parameter*. In the simulations reported below, we vary β across the interval $[0, 0.08]$ using 100 equally spaced values.

The weights are normalized independently within each network. For $X \in \{A, B\}$ and $i \in X$,

$$e_i = \frac{\widetilde{e}_i}{\sum_{j \in X} \widetilde{e}_j}, \qquad \sum_{i \in X} e_i = 1. \tag{6}$$

This independent normalization assigns the same total energy to both competitors. It therefore removes differences in overall energy scale and isolates the effect of how a fixed resource is distributed among the nodes of each network; the within-network spatial heterogeneity is retained. The energy vector used below is $\boldsymbol{e} = (e_1, \ldots, e_{N_T})$.

This choice has two direct implications for the comparison between the two networks. First, the spatial configuration can redistribute energy among the nodes of a network, but it cannot change its total energy. Therefore, a network can only gain an advantage by concentrating its energy on the appropriate nodes, and not by having more energy overall. Without this normalization, moving the nodes of B towards the boundary would also increase the total energy of B, and the effect of its spatial organization would be confounded with a global rescaling of one of the two blocks of M', which, by itself, would favour network B even without any reorganization of its nodes. Second, since all nodes of A are kept at $d_i = 25$ (see above), their normalized energies are uniform, $e_i = 1/N$, and the block of M' associated with network A is simply G_A/N for any value of β. At the reference configuration $s = 0$, the same holds for network B, so that $M' = M/N$ and the outcome of the competition coincides exactly with the purely topological one, independently of β. This provides a natural

Journal Pre-proof

baseline, and every departure from it can be attributed exclusively to the spatial redistribution of energy within network B.

Let

$$E = \mathrm{diag}(e_1, \ldots, e_{N_T}) \tag{7}$$

be the diagonal matrix containing the node energies. We define the *spatially modulated evolution operator*

$$M' = EM, \tag{8}$$

and the linear dynamics of the state vector $\boldsymbol{n}(t)$ is

$$\boldsymbol{n}(t+1) = M'\boldsymbol{n}(t). \tag{9}$$

Note that the operator M' is not a stochastic transition matrix, since its rows or columns do not generally sum to one, and Eq. (9) is not intended to describe a probability-conserving Markov chain. In fact, it represents a linear propagation mechanism. However, we normalize vector $n(t)$ during iteration when its asymptotic composition is evaluated, and the dominant right eigenvector of M' therefore determines the long-time distribution.

The role of E becomes transparent when Eq. (9) is written in components,

$$n_i(t+1) = e_i \sum_{j=1}^{N_T} M_{ij}\, n_j(t). \tag{10}$$

The sum is the total input that node i receives from its neighbours at time t, and e_i is the fraction of this input that node i is able to retain, or exploit. Since e_i multiplies all the contributions arriving at node i, irrespective of the neighbour they come from, it acts as a property of the receiving node rather than of the links or of the emitting nodes. Importantly, the left multiplication by E scales row i of M, so that e_i modulates the contribution accumulated by the receiving node i. In this way we implement our intended mechanism, since we want the distance to the boundary to represent a node-specific capacity to receive, retain, or exploit the propagated quantity. By contrast, right multiplication, ME, would modulate the contribution emitted by each source node, while a symmetric weighting would represent a third process. These are alternative models, but they encode mechanisms different from the one considered here.

Thus, the topology of the coupled system remains unchanged, while the contribution received by each node is modulated by its spatially dependent energy. In this way, the effective evolution operator M' contains both the topological information (through M) and the spatial information (through E). The interlink is fixed only at the structural level and its existence and base weight remain unchanged in M. Nevertheless, the spatial factor acts on the interlink as it does on every other edge. For interlink endpoints $a \in A$ and $b \in B$, the corresponding entries of $M' = EM$ are $(M')_{ab} = e_a M_{ab}$ and $(M')_{ba} = e_b M_{ba}$. Thus, distance modulates effective propagation through both intra- and inter-network links, while leaving the topology and base edge weights in M unchanged.

Journal Pre-proof

Figure 2 illustrates how the spatial configuration parameter s modifies the competition between the two networks. The example corresponds to two Barabási–Albert networks connected through their most peripheral nodes, with $\beta = 0.05$. Network A remains fixed at the centre of its spatial region, whereas the position of the nodes in network B is reorganized according to the value of s. At the reference configuration, $s = 0$, all nodes of network B are located at the same distance from the boundary and the competition is therefore mainly determined by the topological advantage of network A, which remains dominant as it is depicted in Fig. 2(a). Note that the y-coordinate of the nodes is not relevant for the model and, to facilitate the visualization of the results, we have placed nodes equally separated in the y-axis in this example. For negative values of s, the spatial reorganization places the initially most peripheral nodes of network B progressively closer to the boundary. At the extreme configuration $s = -25$, these peripheral nodes occupy the most advantageous spatial positions, while the most central nodes remain farther from the interface. Despite this spatial reorganization, network A continues to dominate (see Fig. 2(b)), showing that improving the spatial position of topologically weak nodes is, in this realization, not sufficient to compensate for the original spectral advantage of A. The opposite situation occurs for positive values of s. As s increases, the most central nodes of network B move progressively closer to the boundary and therefore acquire a larger spatial advantage. At $s = 25$, the nodes with the largest topological relevance are also those occupying the most favourable spatial positions, and this alignment between centrality and proximity to the boundary is sufficient to reverse the outcome of the competition, so that network B becomes dominant (see Fig. 2(c)). This example illustrates the central mechanism explored in the following sections, namely that spatial reorganization can modify, and even reverse, the outcome expected from topology alone when spatial advantage is assigned to structurally important nodes. Note that node sizes in Fig. 2 are proportional to the eigenvector centrality of the effective evolution operator M', not the initial topological centrality. Consequently, nodes that are initially more peripheral may end up having a higher centrality due to the energy weighting in M', and therefore have a larger size in the figure.

2.4. Outcome measures

2.4.1. Accumulated centrality

Let $\boldsymbol{u}_1$ be the dominant right eigenvector of M', associated with its largest eigenvalue λ_1. We choose its non-negative normalization such that $\sum_{i=1}^{N_T}(u_1)_i = 1$. The accumulated centrality of network A is then

$$P_A = \sum_{i \in A}(u_1)_i, \tag{11}$$

with $P_B = 1 - P_A$. Accordingly, $P_A > 1/2$ indicates asymptotic dominance of network A, whereas $P_A < 1/2$ indicates dominance of network B.

Journal Pre-proof

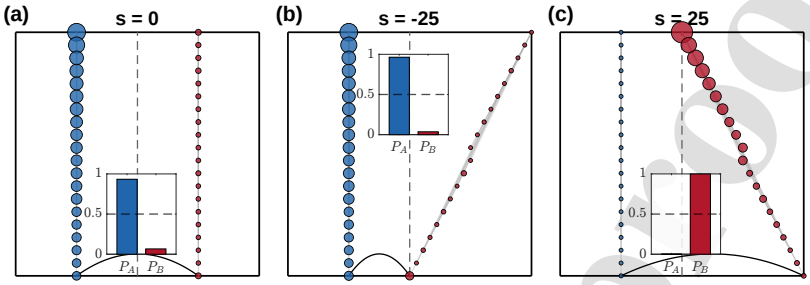

Figure 2: Illustrative effect of the spatial configuration on the competition between two Barabási–Albert networks connected through their most peripheral nodes, for $\beta = 0.05$. Network A remains fixed at the centre of its region, whereas the spatial organization of network B changes with the configuration parameter s. The node size is proportional to their eigenvector centrality in the network-of-networks, derived from the effective evolution operator M'. For visual clarity, we set $N_A = N_B = 20$ in this illustrative example. **(a)** At $s = 0$, network A dominates ($P_A = 0.93$). **(b)** At $s = -25$, the peripheral nodes of B are closest to the boundary and network A remains dominant ($P_A = 0.96$). **(c)** At $s = 25$, the central nodes of B are closest to the boundary and network B becomes dominant ($P_A = 0.01$).

2.4.2. Spatial dispersion of global centrality

To quantify how the dominant eigenvector is distributed in space, we compute a centrality-weighted moment of inertia along an x-axis placed at the centre of mass of the network-of-networks,

$$I_x = \sum_{i=1}^{N_T} (u_1)_i \, (x_i - x_{\mathrm{CM}})^2 \,, \tag{12}$$

where

$$x_{\mathrm{CM}} = \frac{\sum_{i=1}^{N_T} (u_1)_i x_i}{\sum_{i=1}^{N_T} (u_1)_i} \tag{13}$$

is the centrality-weighted centre of mass. Large values of I_x indicate that global centrality is distributed across spatially separated nodes, whereas small values indicate stronger spatial localization.

2.4.3. Time to equilibrium

If we consider that the effective evolution operator M' describes a dynamical process occurring on the network, the time to equilibrium can be obtained by iterating Eq. (9) [7]. At each iteration, the state vector of the whole system is normalized by its Euclidean norm,

$$\widehat{\boldsymbol{n}}(t) = \frac{\boldsymbol{n}(t)}{\|\boldsymbol{n}(t)\|_2}, \tag{14}$$

and compared with the dominant eigenvector $\widehat{\boldsymbol{u}}_1$, normalized in the same way. We define the distance to equilibrium as

$$\Delta(t) = \|\widehat{\boldsymbol{n}}(t) - \widehat{\boldsymbol{u}}_1\|_1 \,. \tag{15}$$

Journal Pre-proof

The equilibrium time t_ε is the first iteration for which $\Delta(t) < \varepsilon$, with $\varepsilon = 10^{-4}$.

A first-order spectral approximation is [31, 7]

$$t_\varepsilon \approx \frac{\ln|\alpha_2^L/\alpha_1^L| - \ln\varepsilon}{\ln|\lambda_1/\lambda_2|}, \tag{16}$$

where λ_1 and λ_2 are the two largest eigenvalues of M' in modulus, and α_1^L and α_2^L are the spectral coefficients of the initial condition obtained from the corresponding left (L) eigenvectors. This approximation makes explicit the role of the separation between the two leading spectral modes in the convergence time.

2.4.4. Analytical analysis of the reversal threshold

Finally, we derived an analytical approximation to interpret the dominance reversal between the two competing networks and estimate its threshold. Since $M' = EM$ is similar to the symmetric operator $S = E^{1/2}ME^{1/2}$, its leading modes are real. Projecting S onto the dominant modes of the two uncoupled spatially weighted networks gives

$$H_{\text{eff}} = \begin{pmatrix} \Lambda_A & \kappa \\ \kappa & \Lambda_B \end{pmatrix}, \tag{17}$$

Here H_{eff} is the 2×2 effective operator obtained by projecting the full symmetric operator S onto the two-dimensional subspace spanned by the dominant Perron modes of the isolated weighted networks. It therefore acts on the amplitudes of these two network-supported modes, rather than directly on the $2N$ individual nodes. Its diagonal elements, Λ_A and Λ_B, are the effective spectral strengths of networks A and B, respectively, while the off-diagonal element κ measures the coupling between their dominant modes through the interlinks.

More explicitly, if $\boldsymbol{v}_X$ is the normalized Perron eigenvector of the isolated weighted block associated with network $X \in \{A, B\}$, then $c_X = \mathbf{1}_X^T E^{1/2}\boldsymbol{v}_X$. Thus, c_A and c_B are scalar conversion factors that measure the total contribution of the isolated modes of networks A and B, respectively, to the right eigenvector of the original asymmetric operator $M' = EM$. Here $\mathbf{1}_X$ denotes the indicator vector of network X, so that the multiplication by $\mathbf{1}_X^T$ sums the components belonging to that network. These factors are required because the accumulated centralities P_A and P_B are sums of the components of the right eigenvector of M', whereas the two-mode projection is formulated using the eigenvectors of the symmetric operator S. With these definitions, the balance condition $P_A = P_B$ reduces to (see the Supplementary Information for the complete derivation)

$$\Lambda_A - \Lambda_B = \kappa\frac{c_B^2 - c_A^2}{c_A c_B}. \tag{18}$$

Equation (18) implicitly defines the analytical reversal threshold s_c^{ana} for each realization and value of β. It predicts that a larger initial topological disadvantage requires a larger spatial displacement and that stronger spatial sensitivity

Journal Pre-proof

reduces the required displacement. The same two-mode approximation gives an avoided-crossing gap, explaining why the transfer of accumulated centrality coincides with the long transients observed numerically.

The two-mode reduction neglects the components of the dominant eigenvector along the remaining eigenmodes of the isolated weighted networks. Standard Rayleigh–Ritz and perturbation arguments [32, 33] indicate that it is most accurate when (i) the leading eigenvalue Λ_X of each isolated weighted network is well separated from the rest of its spectrum, and (ii) the coupling between the leading modes and the omitted ones, which is mediated by the interlink, is small compared with this spectral gap. For a single interlink joining nodes $a \in A$ and $b \in B$, the coupling between the two leading modes is

$$\kappa = \sqrt{e_a e_b}\,(\boldsymbol{v}_A)_a\,(\boldsymbol{v}_B)_b, \tag{19}$$

whereas the coupling between $\boldsymbol{v}_A$ and any other eigenmode $\boldsymbol{w}$ of the isolated network B is $\sqrt{e_a e_b}\,(\boldsymbol{v}_A)_a\,w_b$ (and analogously for the omitted modes of A). Hence, the relative weight of the omitted modes is controlled by the ratio between the components of the connector nodes in the omitted and in the leading eigenvectors, e.g. $|w_b|/(\boldsymbol{v}_B)_b$. In the CC strategy, the connectors are the nodes with the largest Perron components, this ratio is small, and the reduction is expected to be very accurate. In the PP strategy, the connectors are the nodes with the smallest Perron components. Consequently, κ is small, the interlink acts as a narrow spectral bottleneck, and the omitted modes, in which peripheral nodes may carry comparable or even larger components than in the Perron mode, contribute relatively more to the eigenvector of the coupled system. Moreover, according to Eq. (17), the mixing between the two leading modes takes place when $|\Lambda_A - \Lambda_B|$ is of the order of κ. The small value of κ in PP coupling therefore compresses the transfer of centrality into a narrow interval of s, making the location of the transition more sensitive to the neglected contributions. For these reasons, the two-mode approximation is expected to be less accurate for PP than for CC coupling, and its accuracy should also decrease when the spectral gap of the isolated weighted networks becomes small or when several interlinks increase the coupling to the omitted modes.

2.5. Numerical simulations

We perform simulations using pairs of Barabási–Albert networks [34], each with $N_A = N_B = 100$ nodes and an attachment parameter $m = 2$. For every realization, two isolated networks are generated and labelled as A and B so that $\lambda_{A,1} > \lambda_{B,1}$. For each pair, we construct the CC and PP coupled systems and evaluate the complete set of spatial configurations $s \in [-25, 25]$, with a step $\Delta s = 0.5$, over the explored range of β. Results are averaged over 100 independent network pairs. Note that a new pair of networks is generated in every realization, so that the results do not correspond to a single fixed pair of networks, but to an ensemble of 100 independent pairs. The network size is kept fixed at $N = 100$ in order to separate the effect of space from finite-size effects. Instead, the generality of the results is assessed by changing the network

Journal Pre-proof

model, the connector strategy, the number of interlinks, and the energy decay function (see Supplementary Information). For every combination of connector strategy, s, and β, we compute the accumulated centrality P_A ($P_B = 1 - P_A$), the spatial dispersion I_x, and the equilibrium time t_ε. To assess the generality of our findings, we performed an analogous analysis using Erdős–Rényi and Watts–Strogatz network topologies. The corresponding results are provided in the Supplementary Information. The complete set of simulation settings is summarized in Table 1.

Table 1: Summary of the simulation settings used in the main text.

Network model	Barabási–Albert, $N_A = N_B = 100$, $m = 2$
Realizations	100 independent network pairs (a new pair per realization)
Labelling	A (strong) and B (weak) such that $\lambda_{A,1} > \lambda_{B,1}$
Connectors	One interlink; CC or PP, selected with the eigenvector centrality of the isolated networks
Spatial domain	$[0, 100] \times [0, 100]$, boundary at $x_b = 50$
Network A	All nodes at $x = 25$ ($d_i = 25$)
Spatial parameter	$s \in [-25, 25]$, $\Delta s = 0.5$ (101 values)
Energy	$\widetilde{e}_i = \exp(-\beta d_i)$, normalized within each network
Energy parameter	$\beta \in [0, 0.08]$, 100 equally spaced values
Dominant eigenvector	Leading right eigenvector of M', normalized to unit sum
Equilibrium time	Tolerance $\varepsilon = 10^{-4}$; initial condition with uniform values within each network (0.5 and 0.5 per node, respectively); at most 10^6 iterations
Threshold analysis	$\beta \in \{0.03, 0.05, 0.07\}$; s_c from linear interpolation of the crossing $P_A = 1/2$

3. Results

We will investigate how, departing from the classical central–central and peripheral–peripheral connection strategies, networks can take advantage of having the connector nodes close to the boundary. As explained in the previous section, positive values of s correspond to spatial configurations in which the central nodes of the weak network B are moved towards the boundary, whereas negative values correspond to configurations in which its peripheral nodes are moved towards the boundary. First, we will analyse the central–central strategy and then repeat the analysis for peripheral–peripheral coupling.

3.1. Central–central connection strategy

In the CC strategy, the most central node of the strong network A is connected to the most central node of the weak network B. Figure 3 shows the mean of the accumulated centrality P_A over 100 independent realizations as function of the spatial configuration parameter s and the distance-sensitivity parameter β.

Journal Pre-proof

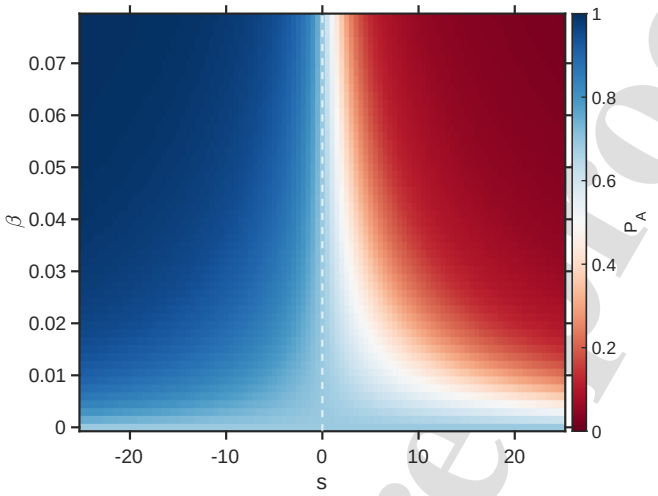

Figure 3: Mean value of the accumulated centrality of network A (P_A) over 100 independent simulations. All networks are constructed using the Barabási–Albert algorithm. We implement a CC connection strategy and analyse the influence of the spatial configuration parameter s and the energy parameter β. The standard deviation across realizations is shown in Fig. S9(a).

The corresponding standard deviation across realizations is shown in Fig. S9(a) of the Supplementary Information. It is low over most of the parameter space and increases only in the vicinity of the transition, where different realizations may be dominated by different networks.

At the reference configuration $s = 0$, similar to Figure 2(a), all nodes of B are located at the middle of their spatial region and we can observe how network A dominates the coupled system, with $P_A > 1/2$. For small values of β, the energy varies only weakly with distance, and network A remains dominant across almost all spatial configurations of B. In this regime, the spatial modulation is too weak to compensate for the initial spectral advantage of the strong network.

The outcome changes when $s > 0$ and β is sufficiently large. In this region, the most central nodes of B are progressively placed closer to the boundary and acquire larger energy values. The mean P_A decreases, passing through an intermediate band around $P_A \simeq 0.5$, and eventually falls below $1/2$, indicating that network B has overtaken network A. For $s < 0$, the central nodes of network B move away from the boundary, whereas its peripheral nodes move closer to it. As a result, network A remains dominant throughout this region of the parameter space: the central nodes of B become progressively weaker as their distance from the boundary increases, while its peripheral nodes do not gain enough energy to compensate for this loss and surpass network A.

Figure 4(a) shows the spatial dispersion I_x of the centrality of the network-of-networks as a function of s and β. The largest values occur near the region

Journal Pre-proof

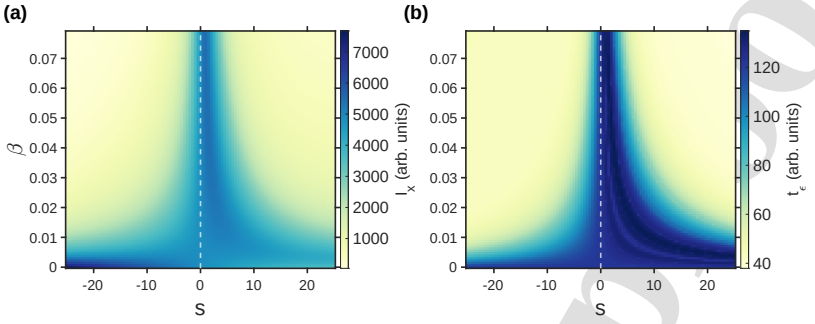

Figure 4: **(a)** Spatial dispersion I_x of global centrality and **(b)** average equilibrium time t_ε as a function of the spatial configuration parameter s and β. Both quantities are averages over 100 simulations of Barabási–Albert networks connected using a CC strategy.

in which the centrality is transferred from network A to network B. There, the dominant eigenvector is distributed across spatially separated parts of the coupled system, placing the centrality-weighted centre of mass between them and increasing the moment of inertia. By contrast, I_x decreases in regions where one network dominates strongly, leading to a spatially localized centrality.

The average time to equilibrium is reported in Fig. 4(b). As in the case of the spatial dispersion, long transients appear where the asymptotic state changes from being concentrated mainly in network A to being concentrated mainly in network B. By contrast, when the configuration of s and β leads to clear dominance by one of the networks, the time to equilibrium decreases. This is especially important in dynamical systems whose intrinsic time scales are slower than, or comparable to, the reported equilibration time.

This coincidence between slow relaxation and the change in accumulated centrality has a direct spectral interpretation. Equation (16) shows that t_ε increases when λ_2 approaches λ_1, provided that the corresponding coefficient of the initial condition is nonzero. The reduced operator in Eq. (17) shows that the same near-degeneracy produces a rapid exchange of the two network-supported components of the dominant mode. It therefore accounts for both the region of long equilibrium times and the transfer from $P_A > P_B$ to $P_A < P_B$.

3.2. Peripheral–peripheral connection strategy

Next, we repeat the analysis for the PP connection strategy, in which the connector link joins the most peripheral nodes (least central) of each isolated network. Figure 5 shows the mean of P_A as a function of the spatial and energy parameters s and β. The corresponding standard deviation is shown in Fig. S9(b) of the Supplementary Information.

The overall organization of the parameter space resembles that of the CC strategy, but the change of dominance is considerably sharper. At $s = 0$, network A displays almost complete dominance. For $s > 0$ and sufficiently large β, the system switches abruptly from $P_A \simeq 1$ to $P_A \simeq 0$ as the central nodes of B

Journal Pre-proof

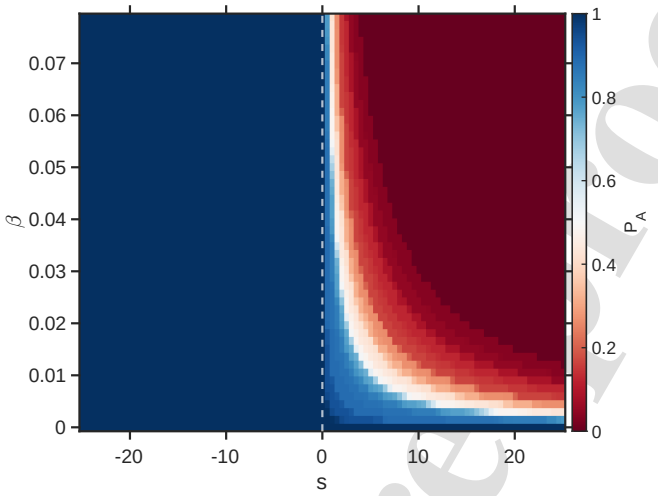

Figure 5: Mean value of P_A over 100 independent simulations of two Barabási–Albert networks connected through a PP strategy. Values of P_A are plotted as functions of the spatial parameter s and the energy parameter β. The standard deviation across realizations is shown in Fig. S9(b).

approach the boundary. Thus, even a connector strategy that strongly favours the initially stronger network can be overcome by a sufficiently strong spatial advantage of the central nodes in B. For $s < 0$, network A remains dominant across the entire parameter space. Consistently with this sharper transition, the standard deviation of P_A under PP coupling reaches larger values than under CC coupling, but within a narrower region of the parameter space (Fig. S9 of the Supplementary Information), a signature of realizations that are dominated by one or the other network.

It is worth noting what happens in the region of the parameter space where the average centrality is approximately balanced between the two networks, i.e., $P_A \simeq P_B \simeq 0.5$. The values of P_A shown in Figs. 3 and 5 are obtained by averaging over 100 network realizations and, therefore, do not necessarily represent the behaviour of each individual realization. This distinction becomes particularly relevant for the PP strategy, whose abrupt behaviour introduces qualitative differences with respect to the CC strategy. Figure 6 shows the probability distribution functions of P_A for the CC and PP strategies for three different combinations of s and β, all of them leading to an average value $P_A \simeq 0.5$, corresponding to the white regions in Figs. 3 and 5. The representative configurations shown in Fig. 6 were selected through visual inspection of the transition boundary across the parameter space, focusing on regions where the average value approaches $P_A \simeq 0.5$. Although the ensemble-averaged values of P_A are close to 0.5 in all cases, the underlying probability distributions are

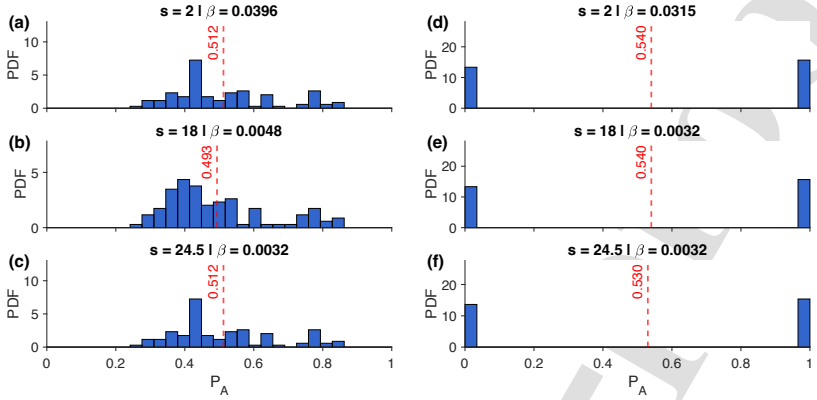

Figure 6: Probability distribution functions (PDFs) of the accumulated centrality of the strong network P_A for the CC (left) and PP (right) strategies when $P_A \simeq 0.5$. (a-c) Distributions obtained using a CC strategy for different configurations: (a) $s = 2.0$, $\beta = 0.0396$; (b) $s = 18.0$, $\beta = 0.0048$; and (c) $s = 24.5$, $\beta = 0.0032$. (d–f) Distributions obtained using PP strategy for different configurations: (d) $s = 2.0$, $\beta = 0.0315$; (e) $s = 18.0$, $\beta = 0.0032$; and (f) $s = 24.5$, $\beta = 0.0032$. The red dashed lines indicate the average value of P_A, all of them close to 0.5.

markedly different. In the CC case, the values of P_A are smoothly distributed around the average, indicating that most realizations display a genuine sharing of centrality between the two networks. By contrast, in the PP strategy the distribution is bimodal, revealing a polarized regime in which each realization typically leads to one of the two networks accumulating almost all the centrality of the system. Thus, an average value $P_A \simeq 0.5$ does not necessarily imply a balanced centrality distribution between the networks. In the PP case, it may instead result from an ensemble average over winner-takes-all realizations. This behaviour reflects the abrupt nature of the PP coupling between competing networks, as previously reported in the literature [31, 7].

Figure 7(a) shows the spatial dispersion obtained for the PP strategy. At first sight, its behaviour appears to be different from that observed for the CC strategy (Fig. 4(a)), but this difference is mainly quantitative rather than qualitative. First, it is important to note the different scales used in the two figures. The maximum dispersion reached under the PP strategy is approximately seven times smaller than in the CC case. Thus, all spatial configurations lead to a much lower dispersion of centrality when the networks are connected through peripheral nodes. Nevertheless, a region of slightly higher dispersion can still be identified, shown in blue in Fig. 7(a). Its origin differs from the region with the highest dispersion under the CC strategy. In the PP case, it appears when network B already accumulates almost all the centrality of the system, i.e., $P_B \simeq 1$, but this centrality is still distributed among several nodes of network B. By contrast, in the CC strategy, the largest dispersion occurs close to the transition region, where centrality is shared between nodes belonging to different

Journal Pre-proof

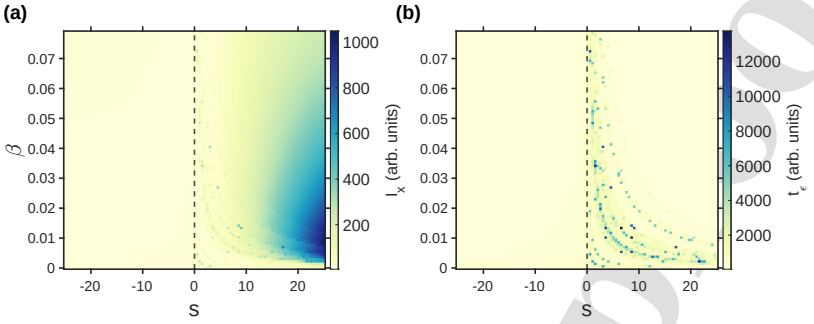

Figure 7: **(a)** Spatial dispersion I_x of global centrality and **(b)** average equilibrium time t_ε as a function of the spatial configuration parameter s and β. Both quantities are averages over 100 simulations of Barabási–Albert networks connected using a PP strategy.

networks. Since the two networks occupy spatially separated regions, sharing centrality across both of them produces much larger values of the spatial dispersion. Therefore, the lower dispersion observed under PP coupling reflects the fact that centrality remains essentially confined within a single network, although, for certain configurations, it can be localized in several nodes.

Finally, the times to reach the equilibrium for the PP strategy are shown in Fig. 7(b). As in the CC case, the longest equilibrium times occur in the narrow transition region where the initially stronger network is no longer able to maintain its dominance over the weaker one (see white regions of Fig. 5). However, unlike the smoother transition observed for the CC strategy, the PP coupling exhibits an abrupt switch between dominance regimes, consistent with the sharp transitions previously reported for PP strategies in the literature [31, 7].

To investigate the interplay between topological asymmetry and the spatial advantage required to overcome it, we examined the relation between the initial difference in spectral strength, $\Delta\lambda_1$, and the critical spatial threshold, s_c. We generated independent network pairs and used the same pair for the CC and PP strategies, thereby preserving identical baseline topologies in the comparison. For each pair, $\Delta\lambda_1$ was calculated before spatial embedding as the difference between the largest eigenvalues of the isolated networks. We then varied s and defined s_c by the crossing $P_A = 0.5$, at which the initially weaker network begins to dominate. This transition was analyzed for three values of β ($\beta = 0.03$, 0.05, and 0.07).

Figure 8 compares the numerical threshold s_c^{num}, with the analytical threshold s_c^{ana} obtained from Eq. (18). In both CC and PP, the two estimates reproduce the positive dependence on $\Delta\lambda_1$ and the decrease of the threshold as β increases. The parity panels show that the reduced model predicts the realization-dependent transition with small error. Across all finite thresholds, the mean absolute errors are 0.063 spatial units for CC and 0.123 for PP (root-

Journal Pre-proof

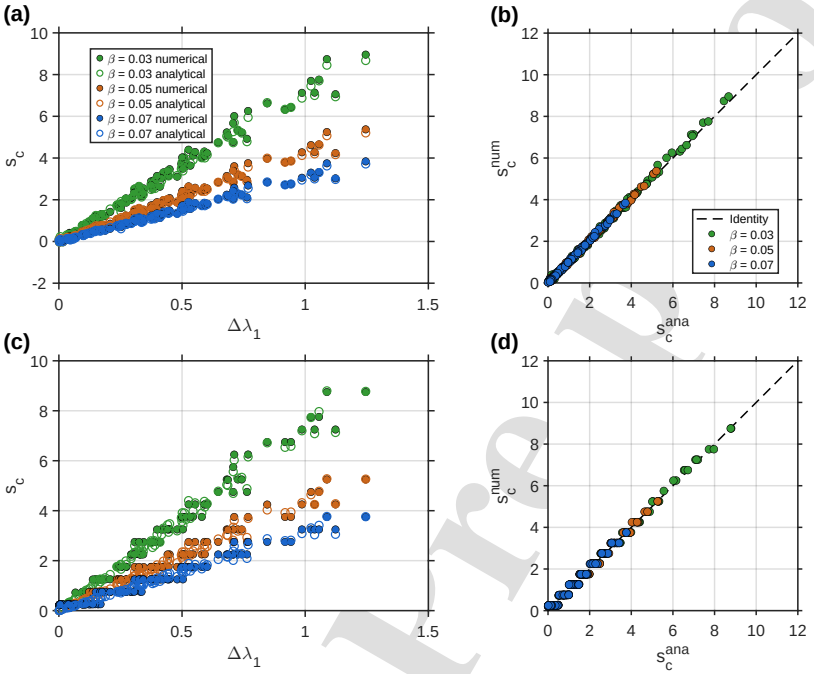

Figure 8: Numerical validation of the analytical threshold. **(a,c)** Numerical thresholds s_c^{num} (filled circles) and analytical thresholds s_c^{ana} from Eq. (18) (open circles) as functions of the initial spectral difference $\Delta\lambda_1$, for CC (a) and PP (c) coupling. **(b,d)** Parity plots comparing s_c^{num} and s_c^{ana} for CC (b) and PP (d). The dashed line denotes exact agreement. Each point represents one of 100 independent network pairs evaluated at $\beta = 0.03$ (green), 0.05 (orange), or 0.07 (blue).

mean-square errors 0.087 and 0.142, respectively). Both mean absolute errors are smaller than the resolution of the s grid, $\Delta s = 0.5$, so that the reduced model locates the transition within the numerical resolution of the simulations for both strategies. The slightly larger PP error is consistent with its sharper, more strongly bottlenecked transition, as anticipated by the validity conditions of the two-mode approximation discussed in Section 2.4.4: in PP coupling the interlink joins nodes with small Perron components, which reduces κ [Eq. (19)] and increases the relative contribution of the omitted modes. Thus, the analytical result quantitatively explains the numerical simulations.

4. Discussion

As we have seen, the spatial organization of networks can reverse the outcome of a competition that would be predicted from topology alone. In the

Journal Pre-proof

absence of spatial heterogeneity, a strong network (here called network A) is expected to dominate because its largest eigenvalue is greater than that of a weaker network (here called network B). However, once the nodes acquire different effective energies according to their distance from a given boundary, this topological advantage could be no longer sufficient to determine the winner. A weaker network can overtake its stronger competitor when its most structurally relevant nodes are placed sufficiently close to the boundary and the dependence on distance is strong enough. Therefore, the outcome of the competition is controlled by an interplay between three elements that cannot be considered independently: (i) the internal topology of each network, (ii) the nodes selected to connect the two systems, and (iii) the spatial position of the nodes with respect to the interface.

This result extends the original competing-networks framework, in which the asymptotic winner is determined by the spectral properties of a network-of-networks and by the centrality of the connector nodes [7, 8]. In the current model, topology continues to play a fundamental role, but its effect is modulated by the energy matrix E. The transformation $M' = EM$ implies that the contribution of each node to the global spectral structure depends not only on its connections (contained in M) but also on its ability to exploit its spatial position (contained in E). In this sense, the relevant quantity is not proximity to the boundary by itself, but the alignment between spatial advantage and topological importance. Bringing the most central nodes of the weaker network close to the boundary is highly effective because spatial advantage reinforces nodes that already have a large structural influence. By contrast, placing only peripheral nodes close to the boundary is generally insufficient, since the energy gained by those nodes does not normally compensate for their weak topological role.

The energy parameter β controls the extent to which spatial location can compete with topology. When β is small, the energy values vary only weakly with distance and the strong network remains dominant almost independently of the spatial arrangement of the weak network. In this regime, the competition is essentially topological. As β increases, proximity to the boundary becomes increasingly important and distinct dominance regions emerge. The transition between these regimes can therefore be understood as a change in the relative importance of topology and geometry. Importantly, the location of this transition is not universal. It depends on the particular network realization, the connection strategy, and the spatial organization of the nodes. This dependence explains the broad regions of increased variance observed close to the change of dominance.

The comparison between the central-central (CC) and peripheral-peripheral (PP) connection strategies further shows that the nodes used to connect the networks affect not only the final outcome but also the nature of the transition between winners. Under the CC strategy, the two most central nodes provide an efficient channel between the networks. As the spatial advantage of the weak network increases, global centrality is transferred progressively from one system to the other, giving rise to a relatively broad transition region. Under

Journal Pre-proof

Journal Pre-proof

the PP strategy, the inter-network connection acts as a much stronger structural bottleneck. The system consequently remains dominated by one network until the spatial advantage of the other becomes large enough to trigger an abrupt reorganization of the leading eigenvector. The transition is therefore much sharper and resembles an almost discontinuous switch between $P_A \simeq 1$ and $P_A \simeq 0$. This observation complements previous results showing that connector nodes determine both asymptotic dominance and transient dynamics in competing networks [7, 8], as well as studies of the transition between localized and delocalized leading eigenvectors in coupled layers [18, 19].

The spatial dispersion provides a complementary description of this reorganization. In the CC case, dispersion is highest close to the region where dominance is transferred from one network to the other. In this regime, a substantial fraction of the global centrality is simultaneously distributed across two spatially separated systems, placing the centrality-weighted centre of mass between them and increasing the corresponding moment of inertia. When one network becomes overwhelmingly dominant, centrality becomes concentrated within a smaller spatial region and the dispersion decreases. The PP strategy reveals a more subtle situation. Its largest dispersion occurs when the spatially favoured network has already gained a competitive advantage but its centrality has not yet collapsed onto a single dominant node. This shows that global dominance and spatial localization are related but are not equivalent. A network may control most of the accumulated centrality while that centrality remains spatially distributed across several of its nodes.

The analysis of the time to equilibrium shows that long transients appear close to the regions where the identity of the dominant network changes. This behaviour is consistent with the spectral expression for the relaxation time, which increases when the two leading eigenvalues become closer and the dominant mode becomes less clearly separated from the subdominant one [31, 35]. The reduced two-mode calculation unifies this dynamical observation with the change of winner: the approach of the two network-supported spectral branches simultaneously narrows the relaxation gap and rotates the dominant eigenvector from one network to the other. More importantly, the analytical balance condition predicts the transition measured with the full operator across individual realizations and all three tested values of β. The small errors in Fig. 8, without fitted analytical parameters, show that the positive relation between initial spectral asymmetry and the required spatial advantage is not merely an empirical linear correlation of the Barabási–Albert ensemble. The approximation is especially accurate for CC coupling and remains quantitatively close for PP coupling, where the sharper transition and stronger inter-network bottleneck increase the effect of modes omitted by the two-dimensional projection.

From the perspective of spatial network theory, the present approach differs from models in which geometry primarily determines whether links can exist or how costly those links are [20, 22, 23, 24]. Here, the topology is kept fixed while space acts directly on the dynamical relevance of individual nodes. This distinction is important. Spatial embedding can affect a network not only by constraining its architecture, transport costs, or connectivity patterns [20, 25],

Journal Pre-proof

but also by changing the effective capacity of nodes that occupy different locations. The energy-vector formulation provides a simple way of introducing this second mechanism into the spectral analysis of competing networks.

Although the present study associates node energy with distance to a physical boundary, the formulation is more general. The components of the energy vector can represent any node-specific property that modifies the ability of a node to accumulate or transmit the quantity involved in the competition. In this broader interpretation, distance is only one possible source of heterogeneity. The same mathematical framework could therefore be used when the relevant advantage is not spatial in a literal sense but can still be represented by a heterogeneous node-dependent factor. This generalization also suggests several natural extensions. A first possibility is to allow the energy vector to evolve in time. Aging or degradation could be represented by a progressive loss of energy in selected nodes, making it possible to study whether spatial reorganization can compensate for the deterioration of structurally important components. A second extension would couple node energy to the dynamical state itself, so that the activity accumulated by a node modifies its future competitive capacity. In such a model, topology, dynamics, and node properties would no longer be separated, as in the broader class of adaptive and coevolving networks [36]. Finally, the network structure itself could become adaptive. Hebbian-like rules, in which interactions are reinforced when pairs of nodes are repeatedly coactivated, provide a natural mechanism for activity-dependent network adaptation in neuronal systems [37]. Related experimental work on neuronal cultures has shown that perturbing synaptic connectivity can trigger large-scale functional strengthening and reorganization, illustrating how network activity and effective connectivity can adapt jointly [38]. These extensions would transform the current static framework into a coevolving system in which spatial position, activity, and connectivity influence one another.

Therefore, a possible application of this type of framework arises in biological and neural systems. Living neuronal networks, for example, provide experimentally accessible systems in which connectivity, collective dynamics, and plasticity can be studied together [39]. Two interacting neuronal populations may be represented as networks occupying different spatial regions and exchanging information through a limited interface. In such a setting, the energy vector need not correspond directly to geometric distance. It could instead encode accessibility to the interface, activity, excitability, or effective coupling strength. Similarly, the two cerebral hemispheres could, at a highly simplified level, be considered as interacting networks whose communication depends on a restricted set of interhemispheric connections. Indeed, previous work explicitly modeled the left and right functional brain networks as competing interconnected subnetworks and showed that the balance of centrality between them depends strongly on the number and distribution of interhemispheric connections [40]. Any application in this direction would require a system-specific definition and empirical calibration of the energy vector, and the present model should therefore be regarded as a conceptual starting point rather than as a direct representation of brain dynamics.

Journal Pre-proof

Journal Pre-proof

The number of interlinks has a non-negligible quantitative effect on the transition. As shown in the Supplementary Information, increasing the coupling multiplicity broadens the region in which accumulated centrality is shared between the networks and makes the transfer of dominance smoother under both CC and PP coupling. Nevertheless, it does not create a qualitatively different dynamical regime and the same topology–space-driven reversal connects the same two dominance states for all tested numbers of interlinks. We note that the comparisons across network models and numbers of interlinks reported in the Supplementary Information are intended as robustness checks of the qualitative mechanism. The quantitative characterization of the transition, including its realization-to-realization variability, is provided for the main BA ensemble through the per-realization thresholds of Fig. 8, the probability distributions of Fig. 6, and the standard deviation maps of Fig. S9. A systematic quantitative comparison of the reversal threshold and of the width of the transition region across network models and coupling multiplicities is an interesting extension of the present work.

On the other hand, several limitations must be considered. The most important is that the energy parameter β, and more generally, the functional dependence between distance and energy, is phenomenological. Different physical, biological, technological, or social systems will have different characteristic spatial scales, and estimating an empirical value of β may be difficult. The exponential decay used here provides a minimal and analytically transparent choice. Although the Supplementary Information shows that the qualitative reversal persists for linear and power-law attenuation, other systems may require threshold, anisotropic, or non-monotonic dependencies. The relative contribution of spatial effects would also have to be calibrated independently for each application. The model otherwise remains deliberately simplified. The robustness tests cover Barabási–Albert, Erdős–Rényi, and Watts–Strogatz ensembles, all four connector strategies, and several interlink multiplicities, but they retain equal network sizes and a fixed straight boundary. Network-size scaling, heterogeneous network sizes, irregular or moving boundaries, several interfaces, and correlations between topology and spatial position remain outside the scope of the present study.

Finally, future work should therefore test the robustness of the results across network sizes, irregular spatial geometries, broader families of energy functions, and more complex coupling architectures. A particularly relevant question is whether the basic mechanism identified here remains valid when topology and spatial location coevolve. The present results suggest that a spatial disadvantage is not necessarily permanent. A topologically weaker system can compensate for its structural weakness by placing the right nodes in advantageous positions. Whether this principle survives under adaptive, nonlinear, and empirically calibrated dynamics represents a natural next step toward a more general theory of competition between spatial networks.

Journal Pre-proof

Journal Pre-proof

Code availability

Custom MATLAB code is available on GitHub (`https://github.com/paularshz/spatial_network_competition`).

Acknowledgments

J.M.B., J.H.M. and P. R.-S. acknowledge the support by Ministerio de Ciencia e Innovación, Spain under grant PID2023-147827NB-I00. All authors thank Jacobo Aguirre for fruitful discussions about competition between networks.

References

[1] S. V. Buldyrev, R. Parshani, G. Paul, H. E. Stanley, S. Havlin, Catastrophic cascade of failures in interdependent networks, Nature 464 (7291) (2010) 1025–1028. doi:10.1038/nature08932.

[2] J. Gao, S. V. Buldyrev, H. E. Stanley, S. Havlin, Networks formed from interdependent networks, Nat. Phys. 8 (1) (2012) 40–48. doi:10.1038/nphys2180.

[3] M. Kivelä, A. Arenas, M. Barthelemy, J. P. Gleeson, Y. Moreno, M. A. Porter, Multilayer networks, J. Complex Netw. 2 (3) (2014) 203–271. doi:10.1093/comnet/cnu016.

[4] S. Boccaletti, G. Bianconi, R. Criado, C. I. del Genio, J. Gómez-Gardeñes, M. Romance, I. Sendiña-Nadal, Z. Wang, M. Zanin, The structure and dynamics of multilayer networks, Phys. Rep. 544 (1) (2014) 1–122. doi:10.1016/j.physrep.2014.07.001.

[5] O. Artime, B. Benigni, G. Bertagnolli, V. d'Andrea, R. Gallotti, A. Ghavasieh, S. Raimondo, M. De Domenico, Multilayer Network Science: From Cells to Societies, Elements in the Structure and Dynamics of Complex Networks, Cambridge University Press, Cambridge, 2022. doi:10.1017/9781009085809.

[6] O. Artime, M. Grassia, M. De Domenico, J. P. Gleeson, H. A. Makse, G. Mangioni, M. Perc, F. Radicchi, Robustness and resilience of complex networks, Nat. Rev. Phys. 6 (2) (2024) 114–131. doi:10.1038/s42254-023-00676-y.

[7] J. Aguirre, D. Papo, J. M. Buldú, Successful strategies for competing networks, Nat. Phys. 9 (4) (2013) 230–234. doi:10.1038/nphys2556.

[8] J. M. Buldú, F. Pablo-Martí, J. Aguirre, Taming out-of-equilibrium dynamics on interconnected networks, Nat. Commun. 10 (2019) 5314. doi:10.1038/s41467-019-13291-2.

Journal Pre-proof

[9] J. Iranzo, J. M. Buldú, J. Aguirre, Competition among networks highlights the power of the weak, Nat. Commun. 7 (1) (2016) 13273. doi:10.1038/ncomms13273.

[10] J. Iranzo, F. Pablo-Martí, J. Aguirre, Emergence of complex socioeconomic networks driven by individual and collective interests, Phys. Rev. Res. 2 (4) (2020) 043352. doi:10.1103/PhysRevResearch.2.043352.

[11] J. Aguirre, J. M. Buldú, J. Iranzo, F. Pablo-Martí, Global multipolarity through the lens of network science and game theory, npj Complexity 3 (1) (2026) 19. doi:10.1038/s44260-026-00082-2.

[12] M. M. Danziger, I. Bonamassa, S. Boccaletti, S. Havlin, Dynamic interdependence and competition in multilayer networks, Nat. Phys. 15 (2) (2019) 178–185. doi:10.1038/s41567-018-0343-1.

[13] P. Bonacich, Power and centrality: A family of measures, Am. J. Sociol. 92 (5) (1987) 1170–1182. doi:10.1086/228631.

[14] T. Martin, X. Zhang, M. E. J. Newman, Localization and centrality in networks, Phys. Rev. E 90 (5) (2014) 052808. doi:10.1103/PhysRevE.90.052808.

[15] R. Pastor-Satorras, C. Castellano, Distinct types of eigenvector localization in networks, Sci. Rep. 6 (1) (2016) 18847. doi:10.1038/srep18847.

[16] R. Pastor-Satorras, C. Castellano, The localization of non-backtracking centrality in networks and its physical consequences, Sci. Rep. 10 (1) (2020) 21639. doi:10.1038/s41598-020-78582-x.

[17] P. Pradhan, A. C.U., S. Jalan, Principal eigenvector localization and centrality in networks: Revisited, Physica A 554 (2020) 124169. doi:10.1016/j.physa.2020.124169.

[18] G. F. de Arruda, J. A. Méndez-Bermúdez, F. A. Rodrigues, Y. Moreno, Universality of eigenvector delocalization and the nature of the SIS phase transition in multiplex networks, J. Stat. Mech. 2020 (10) (2020) 103405. doi:10.1088/1742-5468/abbcd4.

[19] J. Hernàndez Tey, E. Cozzo, Eigenvector localization and universal regime transitions in multiplex networks: A perturbative approach, Phys. Rev. E 114 (1) (2026) 014307. doi:10.1103/6h5q-tv19.

[20] M. Barthélemy, Spatial networks, Phys. Rep. 499 (1–3) (2011) 1–101. doi:10.1016/j.physrep.2010.11.002.

[21] M. Barthélemy, Spatial Networks: A Complete Introduction: From Graph Theory and Statistical Physics to Real-World Applications, Springer, Cham, 2022. doi:10.1007/978-3-030-94106-2.

Journal Pre-proof

Journal Pre-proof

[22] B. M. Waxman, Routing of multipoint connections, IEEE J. Sel. Areas Commun. 6 (9) (1988) 1617–1622. doi:10.1109/49.12889.

[23] J. Dall, M. Christensen, Random geometric graphs, Phys. Rev. E 66 (1) (2002) 016121. doi:10.1103/PhysRevE.66.016121.

[24] M. T. Gastner, M. E. J. Newman, Shape and efficiency in spatial distribution networks, J. Stat. Mech. Theor. Exp. 2006 (01) (2006) P01015. doi:10.1088/1742-5468/2006/01/P01015.

[25] R. G. Morris, M. Barthélemy, Transport on coupled spatial networks, Phys. Rev. Lett. 109 (12) (2012) 128703. doi:10.1103/PhysRevLett.109.128703.

[26] B. Gross, I. Bonamassa, S. Havlin, Dynamics of cascades in spatial interdependent networks, Chaos 33 (10) (2023) 103116. doi:10.1063/5.0165796.

[27] I. Bonamassa, B. Gross, M. Laav, I. Volotsenko, A. Frydman, S. Havlin, Interdependent superconducting networks, Nat. Phys. 19 (8) (2023) 1163–1170. doi:10.1038/s41567-023-02029-z.

[28] J. Coon, C. P. Dettmann, O. Georgiou, Impact of boundaries on fully connected random geometric networks, Phys. Rev. E 85 (1) (2012) 011138. doi:10.1103/PhysRevE.85.011138.

[29] C. P. Dettmann, O. Georgiou, Random geometric graphs with general connection functions, Phys. Rev. E 93 (3) (2016) 032313. doi:10.1103/PhysRevE.93.032313.

[30] P. Expert, T. S. Evans, V. D. Blondel, R. Lambiotte, Uncovering space-independent communities in spatial networks, Proc. Natl. Acad. Sci. U.S.A. 108 (19) (2011) 7663–7668. doi:10.1073/pnas.1018962108.

[31] J. Aguirre, J. M. Buldú, S. C. Manrubia, Evolutionary dynamics on networks of selectively neutral genotypes: Effects of topology and sequence stability, Phys. Rev. E 80 (6) (2009) 066112. doi:10.1103/PhysRevE.80.066112.

[32] G. H. Golub, C. F. Van Loan, Matrix Computations, 4th Edition, Johns Hopkins University Press, Baltimore, 2013.

[33] T. Kato, Perturbation Theory for Linear Operators, 2nd Edition, Springer, Berlin, 1995. doi:10.1007/978-3-642-66282-9.

[34] A.-L. Barabási, R. Albert, Emergence of scaling in random networks, Science 286 (5439) (1999) 509–512. doi:10.1126/science.286.5439.509.

[35] M. Barthélemy, Transitions in spatial networks, C. R. Phys. 20 (4) (2019) 311–317. doi:10.1016/j.crhy.2019.05.002.

[36] T. Gross, B. Blasius, Adaptive coevolutionary networks: A review, J. R. Soc. Interface 5 (20) (2008) 259–271. doi:10.1098/rsif.2007.1229.

Journal Pre-proof

Journal Pre-proof

[37] W. Nicola, C. Clopath, A diversity of interneurons and hebbian plasticity facilitate rapid compressible learning in the hippocampus, Nat. Neurosci. 22 (7) (2019) 1168–1181. doi:10.1038/s41593-019-0415-2.

[38] E. Estévez-Priego, S. Teller, C. Granell, A. Arenas, J. Soriano, Functional strengthening through synaptic scaling upon connectivity disruption in neuronal cultures, Netw. Neurosci. 4 (4) (2020) 1160–1180. doi:10.1162/netn_a_00156.

[39] J.-P. Eckmann, O. Feinerman, L. Gruendlinger, E. Moses, J. Soriano, T. Tlusty, The physics of living neural networks, Phys. Rep. 449 (1–3) (2007) 54–76. doi:10.1016/j.physrep.2007.02.014.

[40] J. H. Martínez, J. M. Buldú, D. Papo, F. De Vico Fallani, M. Chavez, Role of inter-hemispheric connections in functional brain networks, Sci. Rep. 8 (1) (2018) 10246. doi:10.1038/s41598-018-28467-x.

Journal Pre-proof

Journal Pre-proof

Highlights

- We introduce a spatial model for competition between networks across a boundary.
- A weaker network can win when its central nodes lie close to the boundary.
- Node energy encodes distance to the boundary and modulates competition.
- Boundary proximity reshapes the spatial distribution of eigenvector centrality.

Journal Pre-proof

Declaration of Competing Interest

The authors declare that they have no known competing financial interests or personal relationships that could have appeared to influence the work reported in this paper.